MICROSTRUCTURAL ASPECTS OF ZIRCONIA THERMAL BARRIER COATINGS

T.E. Mitchell, D.S. Suhr, R.J. Keller, V. Lanteri, and A.H. Heuer
Department of Metallurgy & Materials Science
Case Western Reserve University
Cleveland, Ohio 44106

Various combinations of plasma-sprayed bond coatings and zirconia ceramic coatings on a nickel-based superalloy substrate were tested by static thermal exposure at 1200°C and cyclic thermal exposure to 1000°C. The bond coats were based on Ni-Cr-Al alloys with additions of rare earth elements and Si. The ceramic coats were various ZrO_2-Y_2O_3 compositions, of which the optimum was found to be ZrO_2-8.9 wt.% Y_2O_3. Microstructural analysis showed that resistance to cracking during thermal exposure is strongly related to deleterious phase changes. Zones depleted of Al formed at the bond coat/ceramic coat interface due to oxidation and at the bond coat/substrate interface due to interdiffusion, leading eventually to breakdown of the bond coat. The 8.9% Y_2O_3 coating performed best because the as-sprayed metastable (high-Y_2O_3) tetragonal phase converted slowly into the low-Y_2O_3 tetragonal plus high-Y_2O_3 cubic-phase mixture, so that the deleterious monoclinic phase was inhibited from forming. Failure appeared to start with the formation of circumferential cracks in the zirconia, probably due to compressive stresses during cooling, followed by the formation of radial cracks due to tensile stresses during heating. Cracks appeared to initiate at the Al_2O_3 scale/bond coat interface and propagate through the zirconia coating. Comparisons have been made with the behavior of bulk ZrO_2-Y_2O_3 and the relationship between the microstructure of the tetragonal phase and the phase diagram. A separate investigation has also been made of the ZrO_2-Al_2O_3 interface.

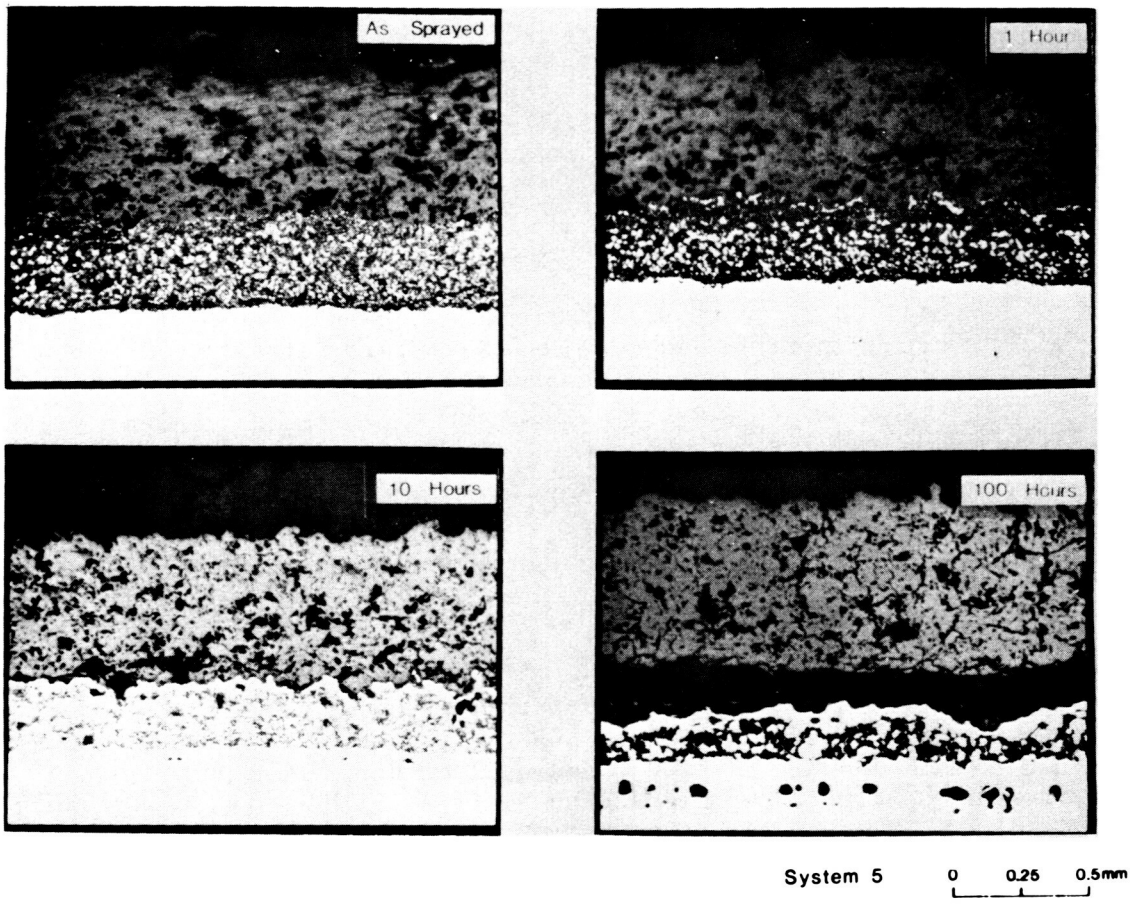

Fig. 1. Optical microstructures of an 8.9% Y_2O_3 system, as-sprayed and after static thermal exposure for 1, 10, and 100 h at 1200°C.

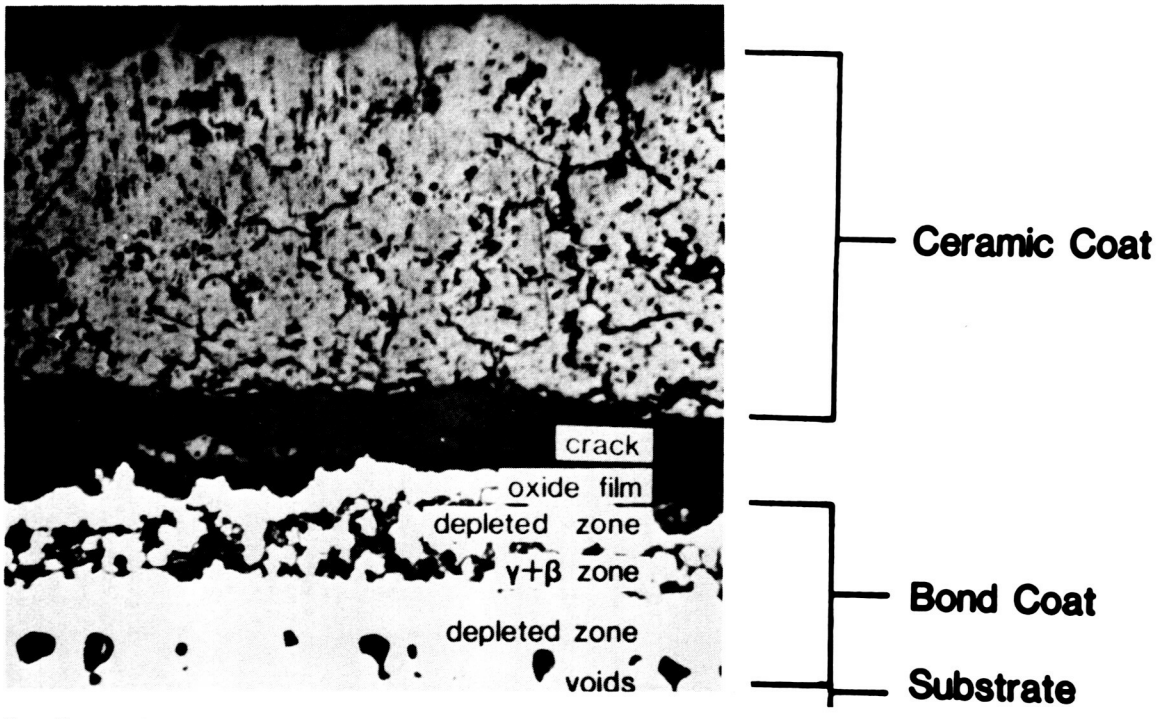

Fig. 2. General optical microstructure of an 8.9% Y_2O_3 system after 100 h static thermal exposure at 1200°C.

Table I. Effect of Y_2O_3 Content in the Ceramic Coat on the Number of 1000°C Cycles to Failure for Individual Specimens with a Given Bond Coat (Ni–Cr–Al with Y and Si Additions)

Y_2O_3 (wt%)	No. of cycles to failure
4.3	7
	15
6.1	233
	233
8.9	>500
	>500
	>500
19.6	321
	>500

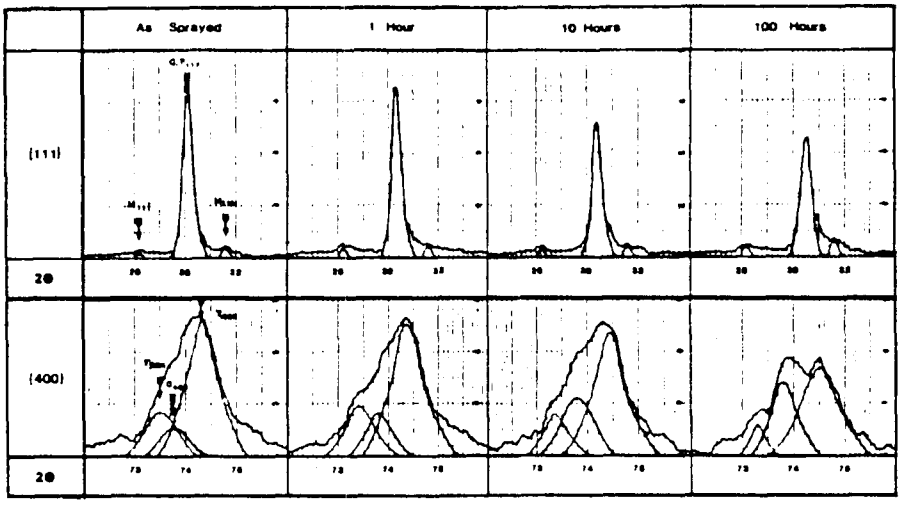

Fig. 3. Experimental X-ray diffraction patterns and deconvoluted peaks in the {111} and {400} regions for plasma-sprayed ZrO_2-8.9% Y_2O_3 after 1, 10, and 100 h static thermal exposure at 1200°C.

Table II. Phase Analyses (mol%) after Thermal Exposure at 1200°C

System (%Y_2O_3)	Phase	Time (h)			
		As-sprayed	1	10	100
4.3	Monoclinic	22	37	41	44
	Cubic	4	5	4	3
	Tetragonal	74	58	55	53
6.1	Monoclinic	16	17	18	20
	Cubic	6	9	10	11
	Tetragonal	78	74	72	69
8.9	Monoclinic	8	9	9	12
	Cubic	13	15	22	31
	Tetragonal	79	76	69	57
19.6	Monoclinic	3	3	2	2
	Cubic	70	76	84	88
	Tetragonal	27	21	14	10

Table III. Chemical Compositions (wt%) in the Bond Coat after Static Thermal Exposure at 1200°C

Time	Al	Si	Cr	Co	Ni	Ti	Phase	Remark
As-sprayed	4.5	2.8	26.9	2.2	63.6		γ/γ'	
	12.7	2.0	15.8	1.7	67.8		β	
1 h	2.5	1.1	19.7	2.8	73.9		γ/γ'	Depleted zone near ceramic coat
	6.1	1.0	11.6	1.9	79.4		β	Below depleted zone
	3.0	1.0	18.5	2.6	74.8		γ/γ'	Below depleted zone
	7.2	0.9	9.1	1.9	80.9		β	Near substrate
	9.9	1.6	17.6	2.7	67.8	0.4	γ/γ'	Near substrate
	2.1	1.4	19.2	3.5	73.3	0.5	γ	Depleted zone near substrate
10 h	2.4	1.2	17.6	4.6	74.2		γ/γ'	Depleted zone near ceramic coat
	3.6	1.8	17.4	4.2	73.0		γ/γ'	Middle of bond coat
	8.5	1.4	9.8	3.8	75.6	0.9	β	Middle of bond coat
	3.4	2.2	17.4	4.8	71.5	0.7	γ/γ'	Depleted zone near substrate
100 h	6.4	2.8	11.4	7.7	70.3	1.5	γ/γ'	Depleted zone near ceramic coat
	7.5	2.4	5.0	4.9	78.4	1.8	β	Middle of bond coat
	5.1	3.6	11.4	8.4	70.8	0.7	γ/γ'	Depleted zone near substrate

Table IV. Chemical Composition (wt%) of the Oxide Film Formed at the Ceramic Coat/Bond Coat Interface

Time at 1200°C (h)	Al_2O_3	Cr_2O_3	CoO	NiO
1	72.6	10.7	0.9	15.8
10	21.8	27.6	2.8	47.8
100	93.1	6.9		

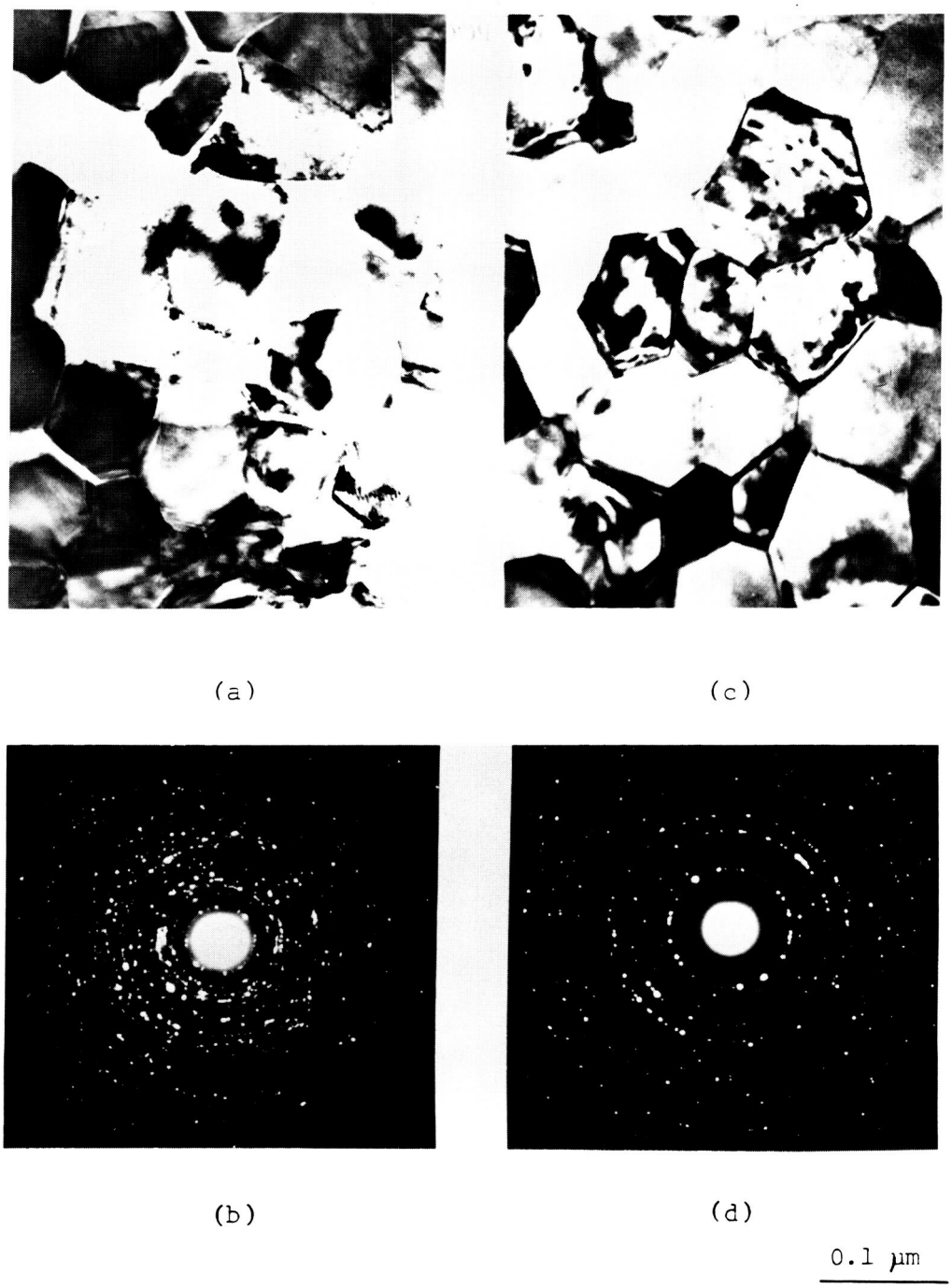

Fig. 4. (a)-(d) TEM micrographs of the as-sprayed 4.3% Y_2O_3 ceramic coating showing the separated regions of monoclinic and tetragonal (T') grains and their SAD ring pattern, (a)-(b) monoclinic ; (c)-(d) tetragonal (T')

0.1 μm

Fig. 5. TEM micrograph of the as-sprayed 6.1% Y_2O_3 ceramic coating showing the non-equilibrium tetragonal $(T')^2$ columnar grains.

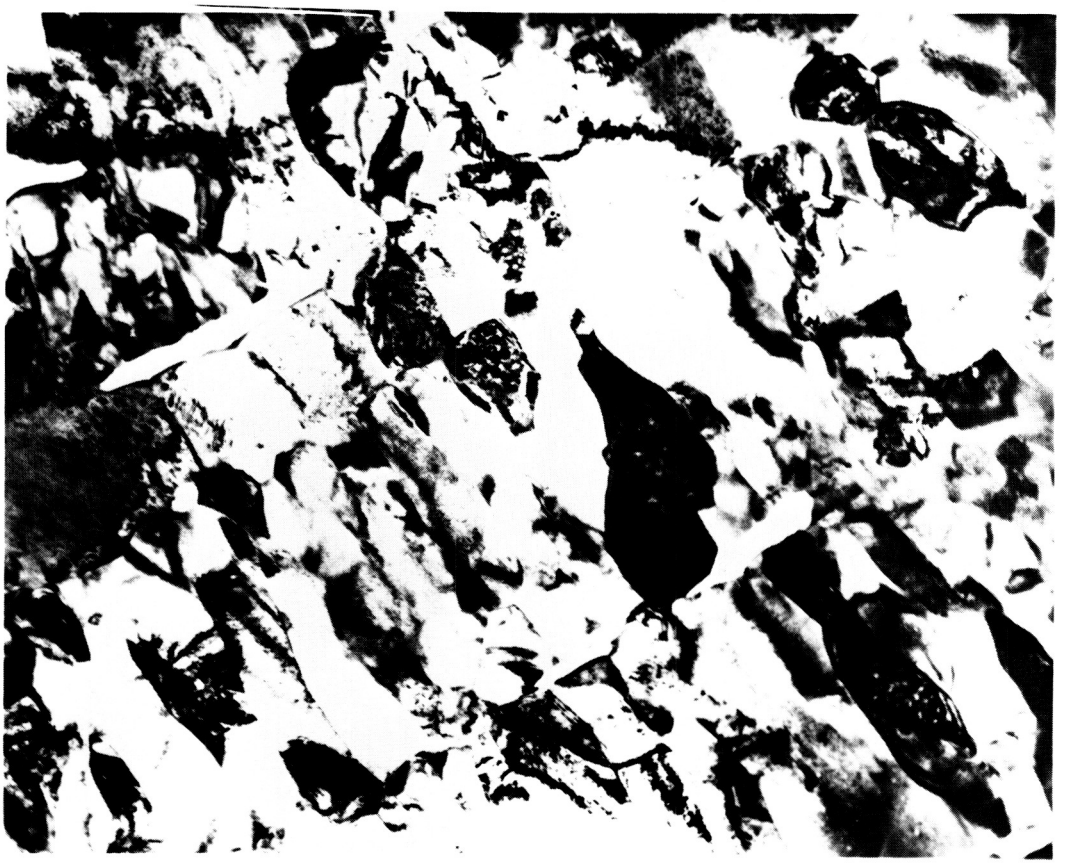

Fig. 6. TEM bright-field image showing the ZrO_2-Y_2O_3 splat morphology with columnar tetragonal grains which have grown perpendicular to the splat boundary (6.1% Y_2O_3) ceramic coat after 100 h at 1200°C.

(a)

0.1 μm

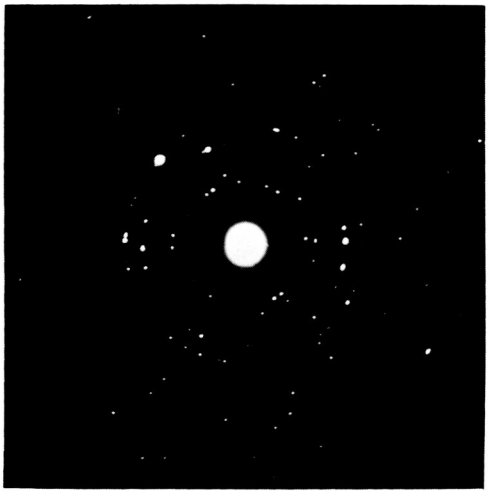

(b)

Fig. 7. (a)-(b) TEM micrograph of the columnar cubic grains within as-sprayed 19.6% Y_2O_3 ceramic coating showing intergranular microcracking (a) and the SAD ring pattern (b).

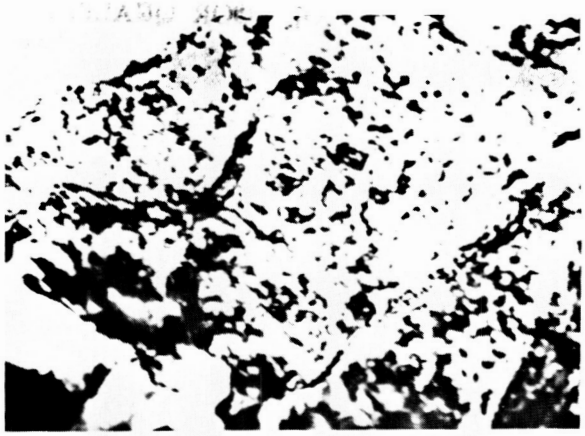

(a)

APB's

0.1 μm

(b)

Mottled
structure

0.1 μm

(c)

Colony
structure

0.1 μm

Fig. 8. (a)-(c) Three kinds of tetragonal phase TEM microstructure

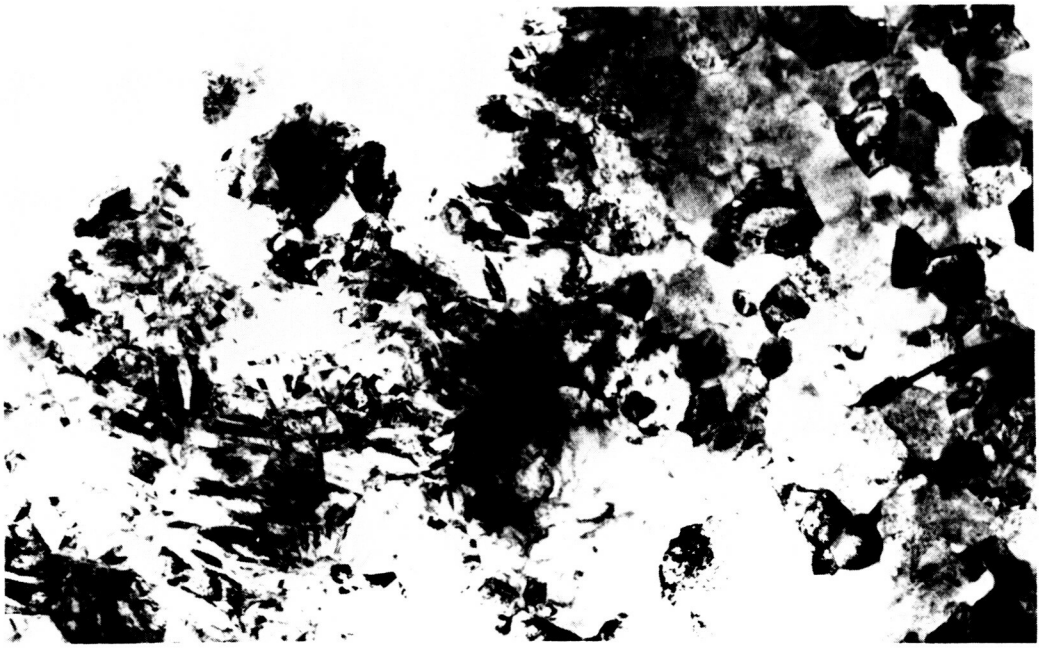

(a)

1 μm

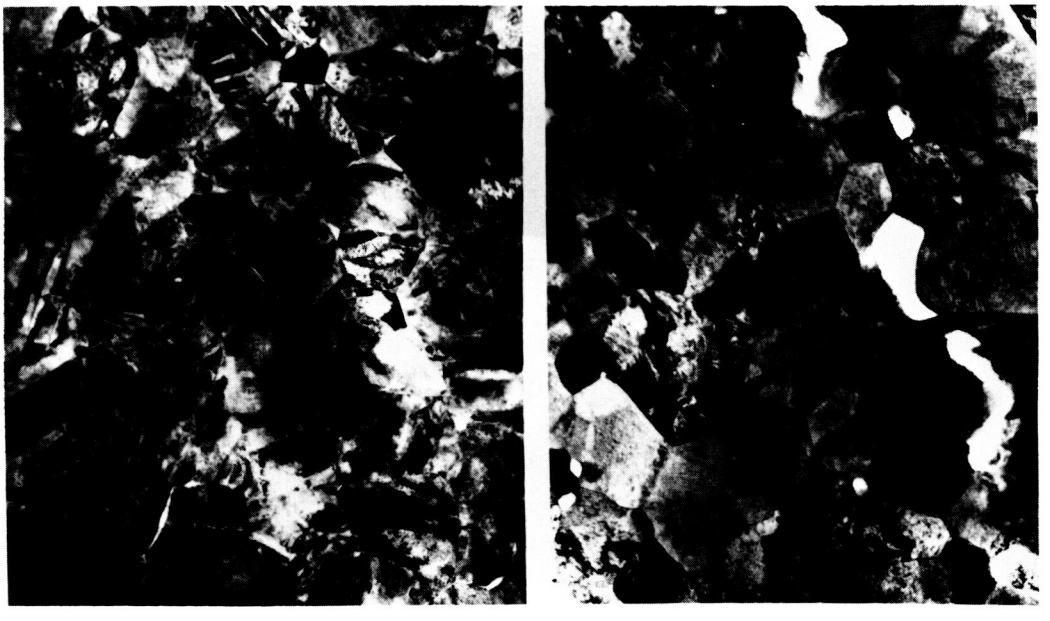

(b)

(c)

0.1 μm

Fig. 9. (a)-(c) 4.3% Y_2O_3 ceramic coating after 100 hours exposure at 1200° C showing separate regions of monoclinic and tetragonal grains.

(a)

0.1 μm

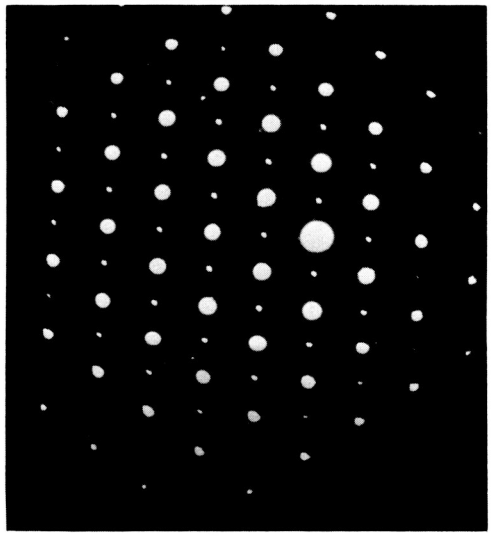

(b)

Fig. 10. 4.3% Y_2O_3 ceramic coating after 100 hours at 1200° C : (a) TEM micrograph of the tetragonal colony structure within large (~ 1.0 μm) grain and (b) corresponding [011] diffraction pattern.

0.2 μm

Fig. 11. 6.1% Y_2O_3 ceramic coating after 100 hours exposure at 1200° C showing splats formed by low Y_2O_3 concentration particle consisting of many twined monoclinic grain and splats formed by high Y_2O_3 concentration particle consisting of tetragonal grains.

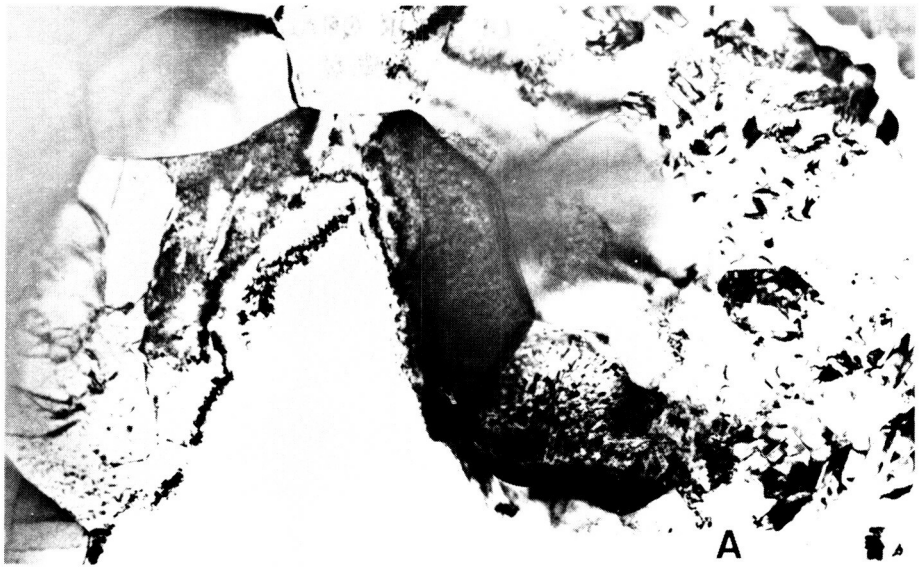

(a)

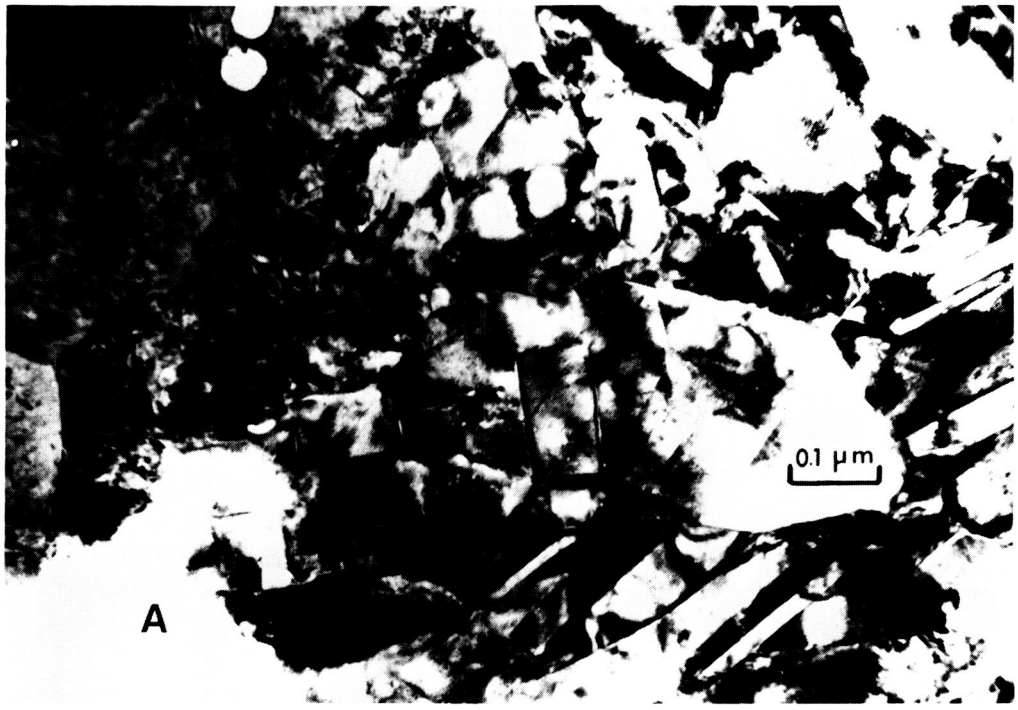

(b)

Fig.12. (a)-(b) 19.6% Y_2O_3 ceramic coating after 100 hours exposure at 1200^{o} C (a) monoclinic and cubic grains (b)higher magnification micrograph showing tetragonal grains(A) formed at the interface between monoclinic and cubic grains due to yttrium diffusion.

0.25 μm

Position	Al_2O_3	SiO_2	Cr_2O_3	CoO	NiO
1	2.2	43.1	9.3	4.3	41.1
2	5.7	55.2	6.9	2.8	29.3
3	25.0	3.3	65.2	0.6	5.8

Fig. 13. TEM micrograph of oxide scale after 1 hour thermal exposure at 1200° C and the result of point EDAX analyses (system 5). The oxide scale is adherent to the bond coating, however pores are present at the oxide scale/ceramic coating interface.

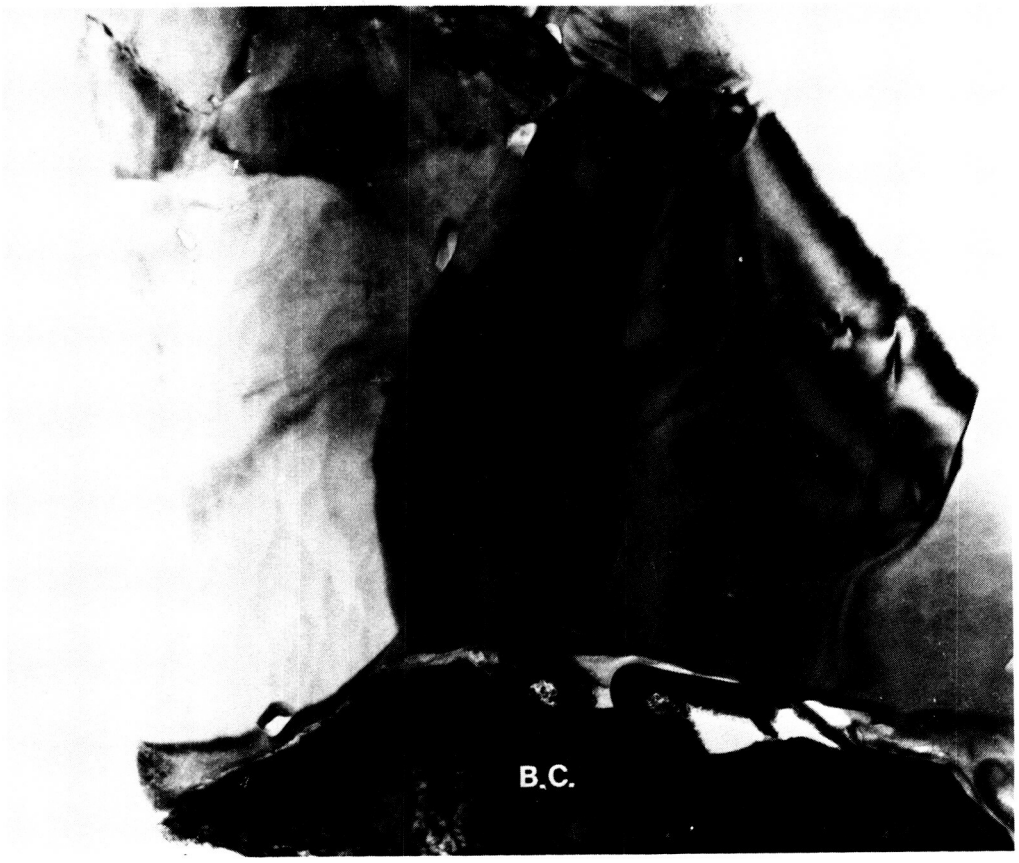

Fig.14. TEM micrograph of oxide film after 10 hours thermal exposure at 1200^{0} C showing the columnar grains of Al_2O_3 and the void formation at the oxide film/bond coating interface.

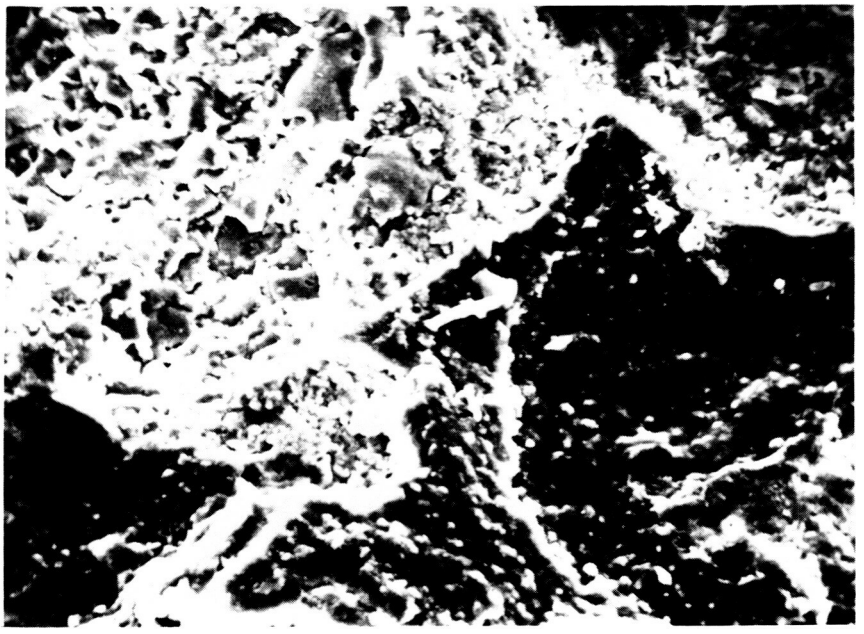

(a)

20 μm

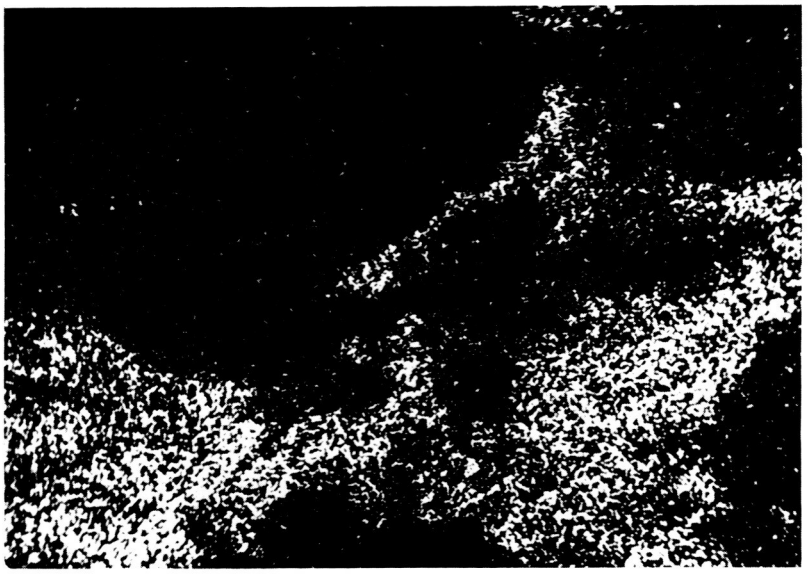

(b)

Fig.15. (a)-(b); (a) SEM micrograph of the bottom-side of ceramic coating (system 10) that had failed after 100 hours exposure and (b) microprobe X-ray map for Al.

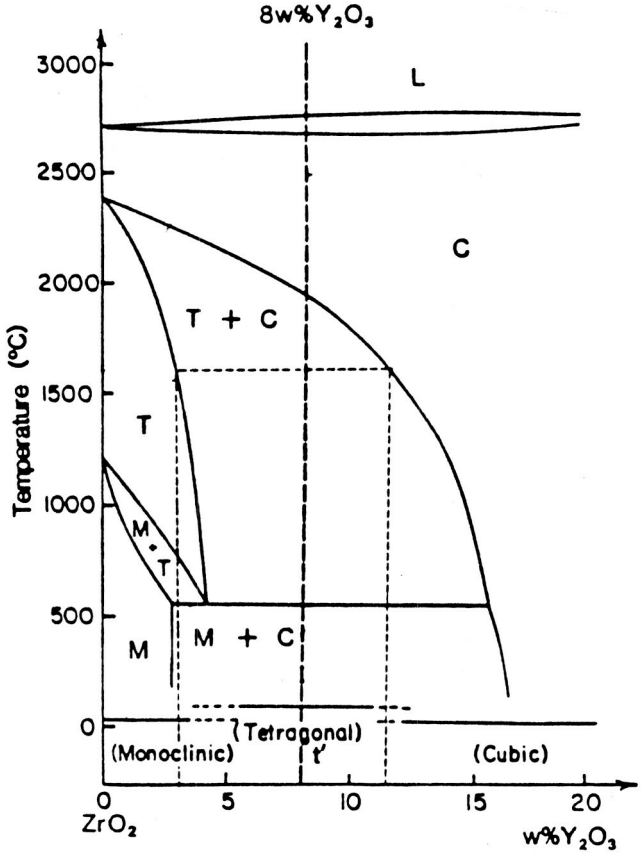

Fig. 16. Phase diagram of the ZrO_2-rich region of the system ZrO_2-Y_2O_3 (Ref. 4).

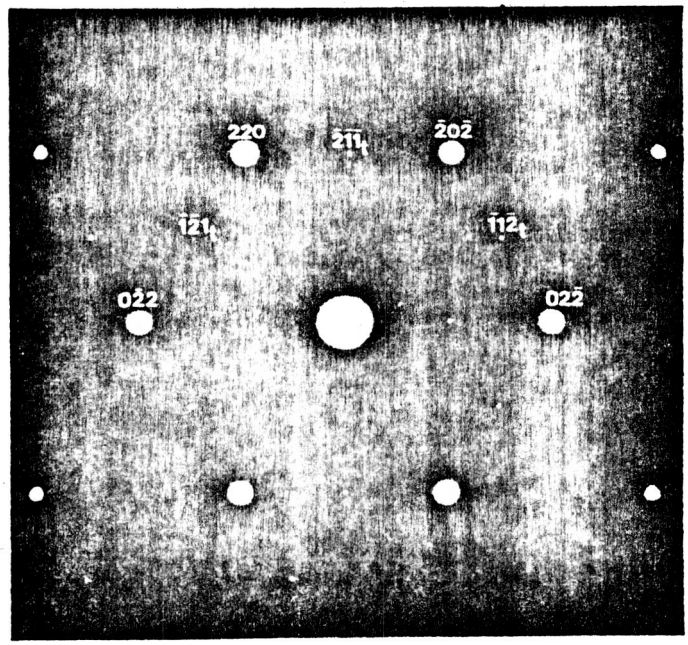

Fig. 17. Diffraction pattern, [$\bar{1}$11] zone axis.

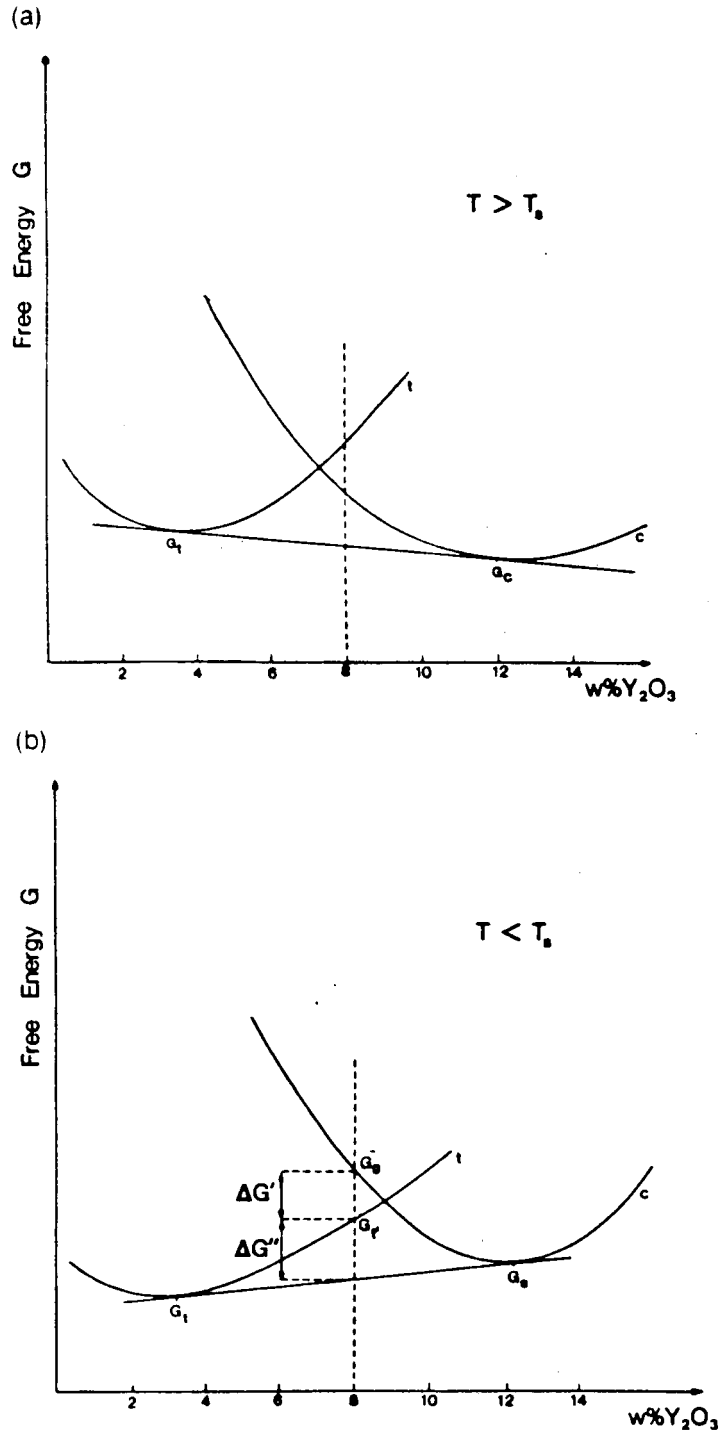

Fig.18. Free energy vs composition curves: (*a*) above the critical temperature T_0 and (*b*) below the critical temperature T_0.